Science Based Design of Weld Metal Microstructure†

Sudarsanam S. BABU*, John M. VITEK* and Stan A. DAVID*

Abstract

There is a need to develop integrated weld process models to predict the properties and performance of welded structures as a function of welding process parameters, alloy composition and service conditions. Such integrated model must couple process, microstructure and structural sub-process models. The first part of the paper will outline ongoing research to develop a problem-solving environment that integrates welding process and microstructure models. The second part of the paper will present on-going research to describe weld metal microstructure evolution in low alloy steel, stainless steel and single-crystal nickel base superalloy welds. The importance of thermodynamic modeling, kinetic modeling, artificial neural network modeling, and characterization techniques will be described.

KEY WORDS: (integrated weld modeling) (solidification) (steels) (stainless steels) (nickel base superalloy single crystals) (problem solving environment)

1. Introduction

The symposium commemorating the 30th anniversary of Joining and Welding Research Institute at Osaka University stresses the importance of establishing a framework for theoretical prediction of welding process behavior and the need to accumulate reliable experimental data supporting the modeling activity[1]. The present paper describes some of the on-going research that proves the value of the above framework for fusion welding of structural alloys. Fusion welding of structural alloys remains the most versatile fabrication process due to its flexibility and ease of use. With the currently existing knowledge base, it is possible to design fusion-welding processes for a wide range of structural alloys and applications. However, the application of fusion welding processes to new structural alloys and new structural designs still require expensive and extensive experimental validation starting with welding consumable design, and process and process parameter optimization. This limitation has been removed by many researchers over the past two decades by developing computational models to predict the arc-weld interactions, pool geometry, microstructure, property and performance of welded structures[2-13]. In addition, numerous analytical models have been developed based on artificial neural network (ANN) methodology[14-16].

Even with remarkable progress made by various researchers throughout the world, there are many challenges that need to be addressed by welding researchers. Most of the computational models developed in the academic literature are not readily accessible to welding engineers and welders. Adding to this shortcoming, the sophisticated models are ever more difficult to use due to the requirement of extensive training and experience in using these models. In the next level, there is no established methodology to incorporate recent advances in the development of process models, microstructure models and performance models in an integrated fashion.

In addition, there is a need to couple solidification and phase transformation theoretical models in a generic model so that it can describe microstructure evolution under varied weld heating and cooling conditions. All the above are needed for design of weld microstructures based on fundamental principles, rather than experimental trial and error.

2. Problem Solving Environment for Weld Process Modeling

Welding processes involve thermo-mechanical-metallurgical interactions. Overriding goals of the

† Received on January 31, 2003
* Materials Joining and NDE Group, Oak Ridge National Laboratory, Oak Ridge, TN 37831-6096, USA

Transactions of JWRI is published by Joining and Welding Research Institute of Osaka University, Ibaraki, Osaka 567-0047, Japan

welding engineer is to describe the above interactions based on prior experience and develop a finished product that meets the required design criteria. In the last decade, Sandia National Laboratory developed the SmartWeld® system that allowed for concurrent model based product and process design for optimizing and manufacturing of welded components[17]. The above approach was extended by Fuerschbach et al[13] to develop optimization software for designing welding process parameters for a wide range of alloys. Supporting the design of the welds final microstructure, a commercial Finite Element Analysis (FEA) code, SYSWELD®, has incorporated methodologies to integrate microstructure evolution through user defined parameters in a kinetic model[18]. In addition, Santella et al[19] used stepwise integration of process, microstructure and structural models to describe the performance of resistance spot-welded structures. However, most of the above models are not easily accessible by the welding engineers due to the level of expertise and training required by the component models. In addition, the above models are not flexible; as a result, the user cannot evaluate the sensitivity of the results to the use of various models that describe either the thermal history as a function of process parameters or the effect of thermal cycles on the microstructure. The models are also difficult to integrate since they were developed on different computer platforms (e.g., Unix, Linux, Windows, and Macintosh) and by different industries, universities and national laboratories. Due to the above reasons, existing integrated welding process tools are usually limited and do not allow for the generic use of a wide range of material and process models.

As an example, an integrated welding process model was developed based on the Problem Solving Environment (PSE) Concept[20]. PSE is a complete, integrated software environment for the computational solution of a particular problem, or class of related problems, that provides an end user with easy-to-use problem solving power based on modular state-of-the-art algorithms, tools, and software infrastructure[21]. In this research, an Internet client-server based approach employing Java® technology as a framework was used. In the first prototype of the PSE system, an integrated model to predict variation of hardness in the weld metal (WM) and the heat-affected-zone (HAZ) of a steel weld was developed. The engineer utilizes the PSE by running a JAVA based client (the PSE-Welding Client) on any computer anywhere in the world.

The client first interacts with a welding-process model that resides within a UNIX server (the PSE-Process Server). This process server is accessed through a set of JAVA servlets that respond to requests from the PSE-Welding client. The PSE-Process Server is based on a welding process model developed with ABAQUS® FEA software for a bead-on-plate geometry. The PSE-Client also interacts with another set of JAVA servlets on a third machine, the PSE-Microstructure Server. These servlets provide access to a microstructure analysis program written in the FORTRAN programming language. The servlets are linked directly to the FORTRAN code through the Java Native Interface. The Fortran code implements a microstructure model that is based on a model developed by Ion et al[3].

The input interface of the welding client is shown in **Fig. 1*a***. After selecting the required parameters, the PSE-Process Server is run first. The PSE-Process Server usually takes 5 to 10 minutes to complete its' calculations. After this step, the PSE-Welding Client obtains thermal histories at different material locations from the PSE-Process Server. When the user clicks on a particular location, the thermal history for that location and the weld composition are transferred to the PSE-Microstructure Server. Using this information, the location's microstructure and hardness are then calculated and the results are transferred to back to the PSE-Weld Client. The results are displayed as shown in **Fig. 1*b***.

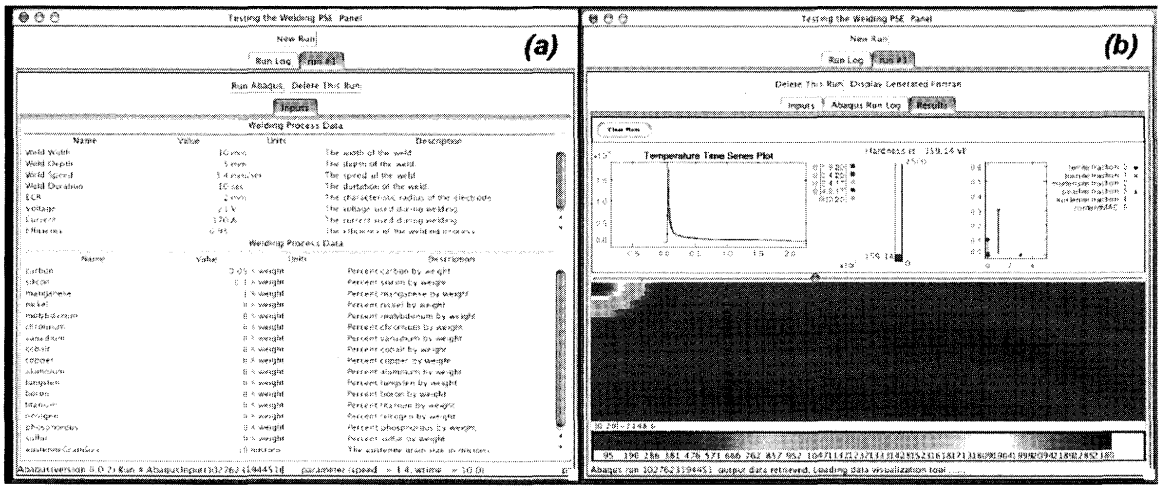

Fig. 1 (*a*) Image of input window of the Welding PSE-Client interface and (*b*)) Image of results window of the Welding PSE-Client interface

In principle, the process and microstructure model can be replaced by models that are more robust, as long as, the input and outputs formats are maintained. Alternatively, analytical models based on ANNs can be used to enhance the speed of calculations.

Although, the above research demonstrated the proposed PSE concept, the research has also highlighted different limitations that need to be addressed in the future. The main issue is that significant model expertise is still needed to address the "errors" that may be generated by component computational models. Another important issue is the need for standardization of the input and output data formats used by different alternative sub-process models. Currently the servlets achieve interoperability by converting component model data into a prototype specific common format. As the system grows, standards will be required so that component models can be readily "plug-replaceable". Functionally, the most important issue is that the integrated model is still limited to serial operations, i.e., the microstructure model and process models are not coupled during solving heat transfer equations. Future research will consider the above limitations. It is noteworthy that the PSE concept also has to deal with software licensing issues when using commercial software codes as component models. However, this can be solved though using a public domain software repository similar to the Materials Algorithm Project[22] or by using a server-supported pay-per-use licensing scheme.

3. Prediction of Weld Metal Microstructure

Even with the development of an integrated weld process model, scientific design of weld microstructure still relies on the availability of generic microstructure models that can describe phase transformations as a function of weld heating and cooling. In this section, ongoing research pertaining to weld microstructure prediction through computational thermodynamics and kinetic models as well as ANNs are illustrated through examples. The focus will be on the application of these models as well as the application of advanced characterization techniques such as in-situ synchrotron diffraction, analytical electron microscopy and orientational imaging microscopy to obtain critical insight into transformation behavior.

3.1 Weld Microstructure Evolution in Fe-C-Al-Mn Steel Welds

During weld solidification of steels, it is known that there is competition between austenite (face centered cubic crystal structure) and ferrite (body centered cubic structure) solidification from the liquid. This phenomenon has been well studied in stainless steel welds. Previous research has shown that in some stainless steels the nonequilibrium austenite phase may solidify first, instead of equilibrium ferrite, at high cooling rates[23-27]. This phase selection phenomenon had been modeled using interface response functions.

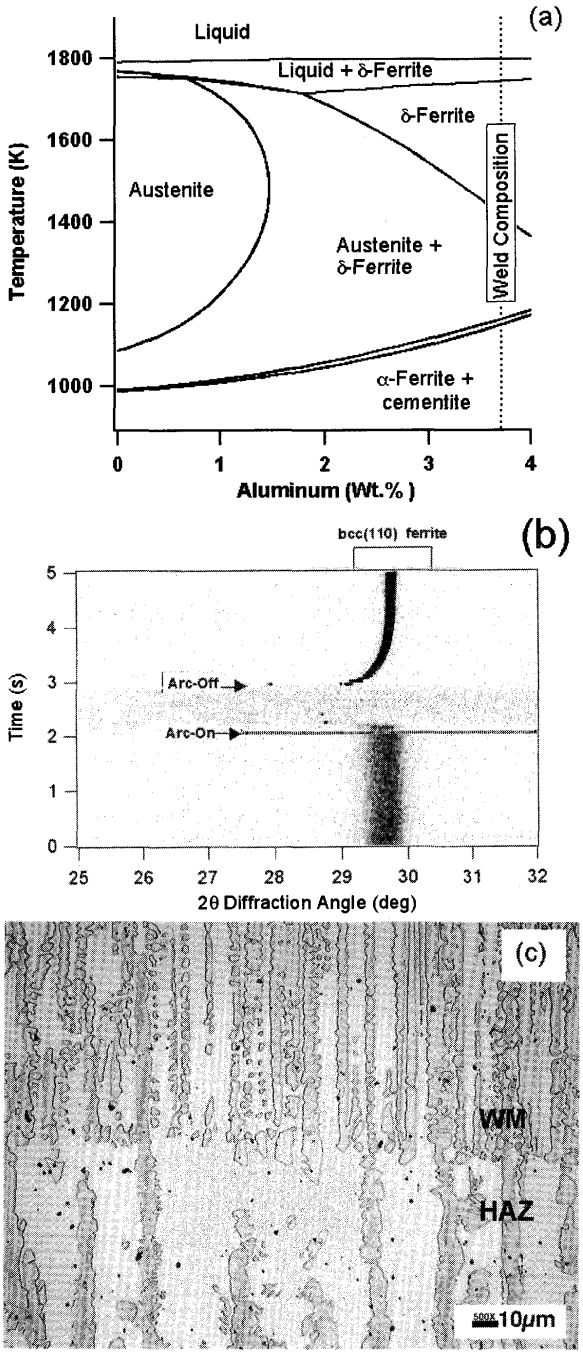

Fig. 2 (*a*) Calculated Fe-C-Al-Mn quasi-binary diagram showing the present weld composition, (*b*) TRXRD results from arc-strike experiment that shows the rapid melting and formation of ferrite (BCC) phase, and (*c*) Optical micrograph showing the transition from HAZ to WM region with an associated reduction in dendrite arm spacing of columnar δ-ferrite in the WM region in the arc-strike experiment

Although, such transitions are expected even in low-alloy steel welds, the interpretation of the final weld microstructure is difficult in those materials due to the low-temperature decomposition of austenite to α-ferrite or martensite. Recent research using a time-resolved X-

ray diffraction (TRXRD) technique with synchrotron radiation such phenomena have been observed in Fe-C-A-Mn steel welds. Under normal weld cooling conditions, the welds containing 1.7 wt.% aluminum solidify as δ-ferrite[28]. The TRXRD observations confirmed this primary δ-ferrite solidification mode and this observation is in agreement with equilibrium thermodynamic predictions. However, under rapid weld cooling conditions, nonequilibrium primary austenite solidification was observed[29]. Calculations using interface response function models showed that the above transition is related to a complex interaction between dissolved aluminum and carbon on the relative stability of liquid, δ-ferrite and austenite[30]. In ongoing work, the above effects are being investigated further by monitoring the phase selection in Fe-C-Al-Mn welds containing 3.7 wt.% aluminum concentrations.

A flux-cored arc weld of Fe - 0.28 C - 0.45 Mn - 0.39 Si – 3.7 Al - 0.004 Ti - 0.003 O - 0.035 N (wt.%) composition was deposited as an overlay on a plain C-Mn steel bar. The aluminum concentration in these deposits is higher than that used in the previous research[30]. A quasi-binary diagram of Fe-C-Al-Mn steel is shown in **Fig. 2*a***. As per the above diagram, the steel with 3.7 wt.% aluminum should always solidify as δ-ferrite. Stationary GTAW (Gas Tungsten Arc Welding) 'spot' welds were made on these weld overlay surfaces by striking an arc on a stationary bar and then terminating this arc after the weld pool had achieved its maximum diameter or after a set hold time. Similar to previous work, rapid or slow cooling rates were achieved by extinction of the arc or a slow slope down of welding current, respectively. In addition, experiments were performed to simulate arc-strike phenomenon, by melting and solidifying within one second on the surface of the sample under the tungsten electrode. In-situ TRXRD measurements were performed during spot welding using the 31-pole wiggler beam line, BL 10-2 at the Stanford Synchrotron Radiation Laboratory with a time resolution of 0.05 and 0.1 second.

Spot welds with slow cooling conditions showed conclusively that initial solidification occurs by δ-ferrite formation. However, with an increase in cooling rate, nonequilibrium austenite solidification was observed. To evaluate this solidification mode change further, the TRXRD measurements were made during an arc-strike experiment. The result is shown in **Fig. 2*b***. The plot shows the bcc (110) diffraction from 0 to 2 s. As soon as the arc was struck at 2-s, rapid melting was observed. During the arc-on time for ~1 s, there was no diffraction

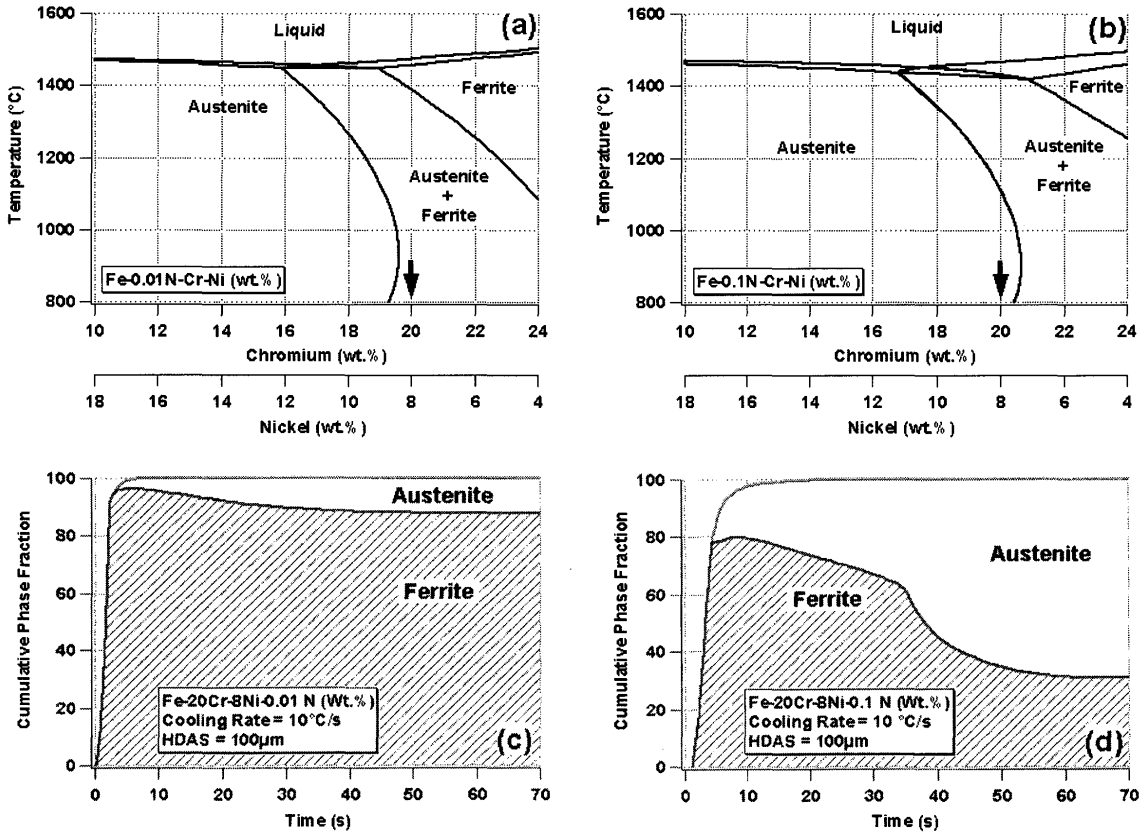

Fig. 3 Quasi-binary diagram showing liquid, austenite and δ-ferrite phase regions in Fe-Cr-Ni alloy systems with (*a*) 0.01 wt.% N and (*b*) 0.1 wt.% N. Calculated variation of phase fraction as a function of cooling time from 1750 K using diffusion controlled growth model for Fe-Cr-Ni alloy systems with (*a*) 0.01 wt.% N and (*b*) 0.1 wt.% N

information, indicating the presence of liquid. With the arc extinction, the diffraction measurements show the appearance of a bcc (110) peak, confirming that the primary mode of solidification in this weld is indeed δ-ferrite. The optical microscopy also confirmed the presence of columnar δ-ferrite [see **Fig. 2*c***]. Interestingly, the reduction in dendrite arm spacing in going from the HAZ in the weld metal region is evident which agrees with the well-known solidification theories. The results show that primary solidification of liquid either to austenite and ferrite is very closely related to interface velocity as well as the complex interaction between aluminum and carbon in the alloy. The research has also shown some difficulties in predicting such phase changes using currently available interface-response function models[30].

3.2 Weld Microstructure Evolution in Stainless Steels

Similar to low-alloy steels, stainless steel weld microstructures are affected by solidification and solid-state transformations. The overall microstructure evolution can be obtained by different computational models. With these models, one can design stainless steel weld metal consumables. This approach will be demonstrated in this section for a hypothetical Fe-20Cr-8Ni (wt.%) alloy with different concentrations of nitrogen. In a first step, one can use computational thermodynamics to obtain a quasi-binary diagram. Such diagrams [see **Fig. 3*a*** and **3*b***] were calculated by using thermodynamic software such as ThermoCalc[31]. The plots show that for alloys with both 0.01 and 0.1 N, the primary solidification will occur by δ-ferrite. In the case of the low nitrogen stainless steel, at 800°C, a mixture of ferrite and austenite is expected. In contrast, for the high nitrogen stainless steel 100% austenite is expected at 800°C. Although, the addition of nitrogen to the present alloy tends to shift towards primary austenite solidification, the primary solidification remains to be δ-ferrite. This is desirable, since the primary austenite solidification increases susceptibility for weld solidification cracking. Such calculations can be used to down select a few alloys for further evaluation. In the next step, one can use diffusion controlled growth models to predict the extent of the ferrite to austenite transformation for a given cooling rate. In this model, the diffusion in liquid, ferrite and austenite are considered with assumed local equilibrium at the interface. Example calculations were performed for the above two alloys. In these simulations, the half-dendrite arm spacing was assumed to be 100 μm and a linear weld-cooling rate of 10 Ks-1 from a temperature of 1750 K was used. The model assumes a peritectic solidification mode. The reader is referred to other publications for more details [23, 32, 33]. The simulations were carried out for the temperature range from 1750 to 1000 K. The variation of phase fraction with time is shown in **Fig. 3*c*** and **3*d***. The results show, in agreement with thermodynamic calculations, the primary solidification phase to be ferrite. The austenite was calculated to grow from the interface of liquid / δ-ferrite interface with subsequent cooling. In the case of the high nitrogen welds, the austenite growth into ferrite phase was found to increase rapidly after ~35 seconds. This time corresponds to cooling of the system below 1135 °C. This temperature corresponds to the temperature below which thermodynamic calculations predict 100% austenite for this composition. Due to the assumption of local equilibrium at the interface, the flexibility of tie line selection and non-uniform composition, the diffusion controlled growth model calculations predict the presence of ferrite even below this temperature. However, the low nitrogen alloy retains a large fraction of ferrite. Thus, the diffusion controlled growth models allow us to calculate the amount of δ-ferrite that may be retained after solidification and to describe the weld microstructure evolution in stainless steels to a certain extent. These calculations can be repeated for different weld cooling rates and dendrite arm spacing to evaluate the effect of welding process parameters on the microstructure.

It is important to note that these calculations cannot be extended to temperatures below 900°C. Below 900°C, only interstitial element diffusion (C or N) is appreciable. As a result, further model that consider paraequilibrium, rather than ortho-equilibrium, is needed[34]. However, this was not done in these calculations. Another important factor in these calculations is the assumed dendrite spacing. One has to rely on experimental measurement or another model for predicting interdendritic arm spacing as a function of composition and cooling rate. Additional complexities may exist in the presence of secondary dendrite arms, which in principle may lead to an apparent change in dendrite arm spacing with an increase in solid fraction. One more limitation is that the model calculates the primary solidification phase based on equilibrium phase diagram. Therefore, we need to couple these models with interface-response function models to allow for nonequilibrium phase selections. The above issues are being addressed in ongoing research[35].

The above models, although based on fundamental phase transformation theories, often become difficult to

Table 1 Range of concentrations (wt.%) for different elements used in the development of ANN for ferrite number prediction

	C	Cr	Ni	Mo	N	Mn	Si	Cu	Ti	Nb	V	Co
Minimum	0.008	14.74	4.61	0.01	0.01	0.35	0.03	0	0	0	0	0
Maximum	0.2	32	33.5	6.85	0.33	12.7	1.3	3.04	0.54	0.88	0.23	0.45

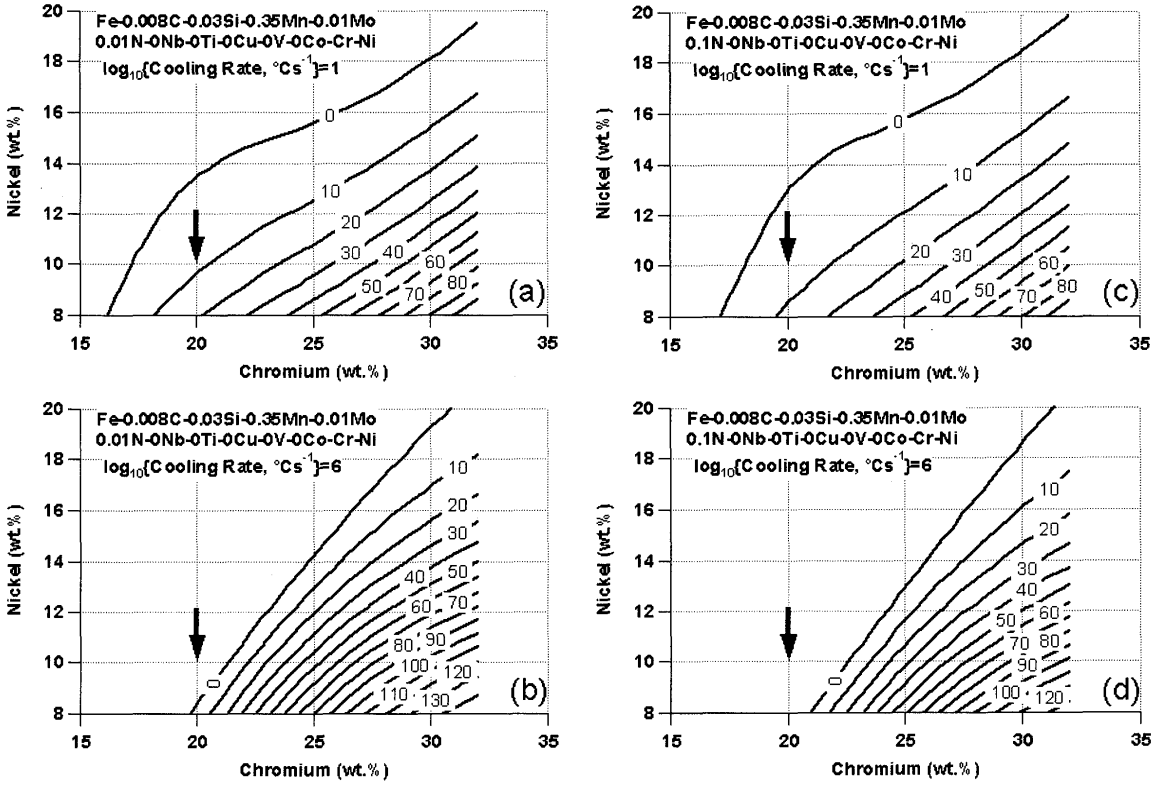

Fig. 4 Calculated contours of ferrite numbers for a stainless steel alloy with 0.01 wt.% N as a function of Cr and Ni concentration at weld cooling rates of (*a*) 10 °C/s and (*b*) 1×10^6 °C/s are shown. Similar plots for a stainless steel alloy with 0.1 wt.% N at weld cooling rates of (*c*) 10 °C/s and (*d*) 1×10^6 °C/s. All the plots were calculated with ORFN model[36].

use when extending them to multicomponent systems (e.g. in a generic stainless system of Fe-Cr-Ni-Mo-Ti-C-N). In addition, the diffusion controlled growth calculations over a wide range of composition becomes very difficult and computationally intensive. Another successful approach has been to use ANNs to map the effect of stainless steel composition and cooling rate based on a large experimental dataset. This was recently performed by Vitek et al[36]. Using experimentally measured ferrite number (FN) from over 1196 welds for a wide range of elemental concentrations (see Table 1) and calculated cooling rates (thin and thick plate conditions) in the range of 10^1 to $10^{6.4}$ °Cs^{-1}, an ANN (ORFN) was developed.

The ORFN model was applied to the hypothetical stainless steel composition considered earlier, i.e., Fe-20Cr-8Ni (Wt.%) alloy. The predicted FN for different Cr and Ni concentrations are plotted in **Fig. 4*a*** to **4*d*** for two different nitrogen levels at slow (10 °C/s) and fast (1×10^6 °C/s) weld cooling rates.

These calculations, however, have to consider some minimum levels of C, Si, Mn, and Mo since the ORFN is trained with these minimum concentrations. The calculations show that with an increase in nitrogen concentration for a slow cooling rate the ferrite number drops from 20 to 10. This trend is consistent with the trends predicted by computational thermodynamic and kinetic calculations. However, when the cooling rate is increased to 1×10^6 °C/s, the FN of 1.7 is predicted for low N welds. Based on prior diffusion controlled growth calculations, this result may appear to be contradictory, i.e., if the weld solidifies as δ-ferrite, with increase in cooling rate, the FN should increase due to less time for growth of austenite into ferrite. However, careful analysis of the ANN calculations indicated that with an increase in cooling rate to 2000 °C/s, the FN increased from 20 to 32. Beyond this cooling rate, the FN dropped with an increase in cooling rate. This reversal is indeed expected, because at higher cooling rates, the change in primary solidification from ferrite to austenite is predicted. As a result, the ferrite content is expected to decrease which is in agreement with interface-response function calculations on similar steels[23]. The plots in Fig. 4 also show that with an increase in nitrogen, 100% austenite microstructure will be obtained more easily. Interestingly, the plots also show a change in phase selection may not occur in high Cr steels, such as duplex stainless steels. This is shown by the increase in FN, and not a decrease at high Cr levels and high cooling rates. The above example illustrates that one can use hybrid models of computational thermodynamics, kinetic and artificial neural network models to design weld microstructures as a function of

composition and cooling rate.

3.3 Microstructure Evolution in Single-Crystal Nickel Base Superalloy Welds

In recent years, there is an increased need to weld single-crystal nickel base superalloys for efficient reuse and repair of failed and rejected components. Fusion welding through gas tungsten arc, electron beam and laser welding are being considered. The focus of the computational modeling in this alloy system is to avoid the formation of stray grains in these alloys during welding, because stray grains promote weld cracking. The second focus of the modeling is to evaluate the solidification range in these alloys, which influence the cracking tendency and the microsegregation. The third focus of the work is to evaluate the partitioning behavior between γ and γ' phases that evolve during subsequent cooling after solidification.

The tendency for stray grain formation is related to the solidification temperature range (ΔT), diffusivity in liquid (D), orientation of single crystal with respect to welding direction, welds pool geometry, and welding velocity. The tendency for stray grain formation arises due to the following phenomena. In a cubic crystal such as that of nickel base superalloys, there is competition between [001], [001], [010], [010], [100], and [100] dendrite growth orientations at different parts of the weld-pool solidification front. Depending upon the relative orientation of the weld-pool solidification front normal with respect to the welding direction, one of the variants will be favored. As a result, the growth velocity (v) of dendrites can be lower or higher than the magnitude of the welding speed at different regions of the weld-pool solidification front. Such changes in the growth velocities for a given set of welding parameters will also lead to widely varying G/v ratios, where G is the temperature gradient ahead of the growing dendrite. Due to this spatial variation of G/v, it is possible to satisfy the condition for increased constitutional supercooling [$(G/v)<(\Delta T/D)$] in some of these regions.

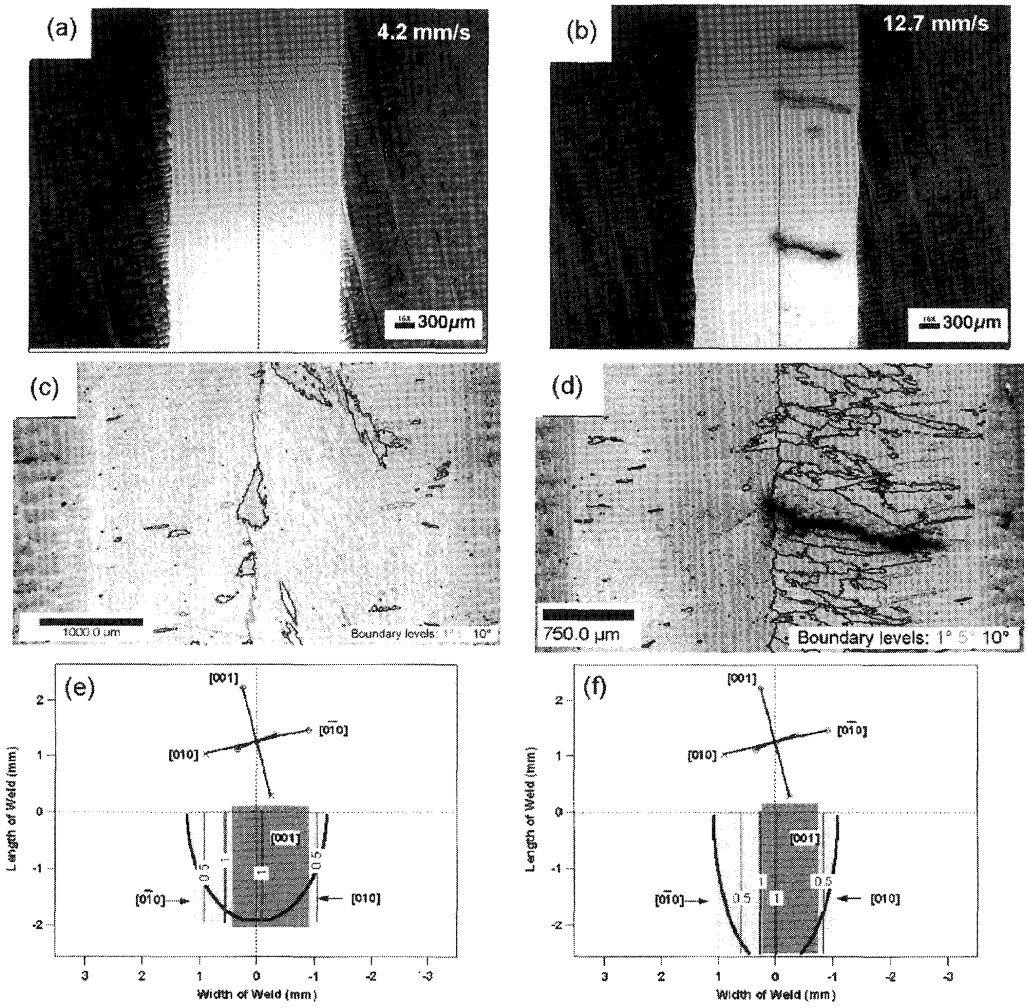

Fig. 5 Optical micrograph of surface of laser welds made on N5 single-crystal nickel base superalloy with welding speed of (*a*) 4.2 mm/s and (*b*) 12.7 mm/s. Orientational imaging microscopy results showing the grain boundary character with welding speed of (*c*) 4.2 mm/s and (*d*) 12.7 mm/s. Predicted dendrite growth selection, crystallographic orientation of the sample and contours of v_{ratio} at different regions of welds with welding speed of (*e*) 4.2 mm/s and (*f*) 12.7 mm/s.

This increased undercooling leads to the nucleation of equiaxed dendrites, i.e., formation of stray grains ijn these welds. It is possible to predict such effects using a geometrical model developed by Rappaz et al [37] and by combining with equiaxed growth models [38, 39] demonstrated by with an example of laser welding of Rene N5 single-crystal nickel base superalloy.

Autogeneous laser welds were made on single-crystal nickel-base superalloy Rene N5 (Ni-0.05C-7.5Co-7Cr-1.5Mo-5W-3.00Re-6.5Ta-0.15Hf) with two different welding speeds (4.2 and 12.7 mm/s). The power level for the low speed was 420 W and that of the high speed weld was 804 W. In this case, using the Laue diffraction technique, the welding direction was found to be [0.141, 0.217, 0.966] and surface normal was [0.925, 0.376, 0.051]. The optical micrographs of the top surface from both welds are shown in **Fig. 5*a*** and **5*b***. The micrograph from the high-speed weld showed extensive cracking only on the right side of the weld and there were no cracks in the low-speed welds. These welds were examined using Orientational Imaging Microscopy (OIM) and the results are shown in **Fig. 5*c*** and **5*d***. The OIM results show that there is large number of high-angle grain boundaries (misorientations greater than 10°) in the right side of the weld at high-speed welds in comparison to that on the left side, or at low speed welds. The geometric model was applied to predict the preferred dendrite growth variant and the ratio (v_{ratio}) of dendrite growth velocity (v_{hkl}) to welding velocity (v_{weld}) for the above condition. The predicted results are shown in **Fig. 5*e*** and **5*f***. The calculations showed that for both conditions, the preferred growth variants are [010], [010] and [001]. The [010] variants grow from the left side of the pool and extend into the weld pool far than [010] variants from the right side of the pool. As a result, the most predominant growth direction on the right side of the pool is [001]. The velocity of these dendrite increases towards the center of the weld pool. Since the absolute values of dendrite growth velocity (v_{hkl}) increases with an increase in welding speed (v_{weld}), there is a greater degree of constitutional supercooling and a high probability of stray grain formation on the right side of the weld pool in high-speed welds. This was confirmed by recent work by Park et al[40] who coupled the results from the geometrical model with thermomechanical calculations for the same conditions. This result again stresses the need for integrated weld process modeling that couples process and microstructure models presented in the earlier section.

The next step in the application of computational modeling for these alloys is to predict the solidification temperature range (ΔT). The solidification temperature ranges can be calculated using multicomponent thermodynamic software[31] and commercial thermodynamic databases[41] assuming Scheil-Gulliver additivitiy law. In this regard, one also has to pay attention to the magnitude of growth velocity. At high growth velocity, ΔT may decrease due to nonequilibrium partitioning of alloying elements between liquid and solid[42, 43]. Nonetheless, in principle, the above can be calculated to describe the tendency for stray grain formation and microsegregation in these alloys.

The final step in the application of the computational model is to describe the decomposition of γ phase into a mixture of γ and γ′ mixture during subsequent cooling. The computational thermodynamic models can be applied to predict the partitioning of alloying elements as a function of temperature and composition. By assuming local equilibrium, and ignoring diffusion in the γ′ phase, it is now possible to predict the growth rate and change in partitioning between γ and γ′ phases during continuous cooling conditions. However, recent work using atom probe tomography has shown that partitioning between γ and γ′ phases can depart from equilibrium to nonequilibrium conditions under large undercooling[44]. Current, on going research focuses on developing computational tools to address this nonequilibrium partitioning.

4. Summary and Conclusions

For scientific design of weld microstructure there is a need to integrate welding process, microstructure and performance models to predict the overall performance of welded structures. An example showing problem solving environment approach, for flexible integration of these models through the Internet, was presented. The importance of a comprehensive weld microstructure model was illustrated with examples from low-alloy steel, stainless steel and single-crystal nickel base superalloy welds. The phase selection during weld solidification in a Fe-C-Al-Mn low alloy steel weld was demonstrated with the in-situ TRXRD technique using synchrotron radiation. The weld microstructure evolution in stainless steels can be predicted to a greater accuracy by using different computational tools including computational thermodynamics, diffusion controlled growth models and artificial neural network models. The added complexity of weld microstructure evolution in single-crystal alloys due to crystallographic constraints was highlighted. Non-symmetric stray grain formation and associated weld cracking was observed in a commercial single-crystal nickel base superalloy during autogeneous laser welding along a high-index crystallographic direction. The above weld microstructure evolution was explained with a geometric model for dendrite growth selection and constitutional supercooling theory.

Acknowledgements

The research was sponsored by the Laboratory Directed Research and Development Program of Oak Ridge National Laboratory (ORNL), Division of Materials Science and Engineering, and Advanced Power—Turbine Systems Program, Office of Fossil Energy, U. S. Department of Energy—National Energy Technology Laboratory, under contract number DE-AC05-00OR22725 with UT-Battelle, LLC. The authors

thank Ms. Marie Quintana from Lincoln Electric, Prof. D. Walker of University of Cardiff, UK, Drs M. Summers, G. Sarma and M. L. Santella from ORNL, Drs. J. W. Elmer and T. Palmer from Lawrence Livermore National Laboratory and Dr. J. W. Park from UT/ORNL for collaboration in the research described in this paper. The authors acknowledge Drs Q. Han and J. W. Park for valuable discussions.

References

1) Proceedings of symposium on "Joining and Welding Solution to Industrial Innovation," held at Osaka University, Japan on March 14, 2003
2) S. A. David and T. DebRoy: *Science*, **257** (1992), p. 497.
3) J. C. Ion, K. E. Easterling, and M. F. Ashby: *Acta Metall.*, **32** (1984) p. 1949
4) S. Kou and Y. H. Wang: *Metall. Trans. A.,* **17** (1986) p. 2265
5) A Kar and J. Mazumder: *J. Appl. Physics*, **78** (1995) p. 6353
6) K. Mundra, T. DebRoy and K. M. Kelkar, *Num. Heat Transfer Part A – Applications*, **29** (1996) p. 115
7) T. Zacharia, S. A. David, J. M. Vitek and T. DebRoy: *Welding Journal*, **68** (1989) p. 499s
8) J. Goldak, A. Chakravarti, and M. Bibby: *Metall. Trans. B*, **15** (1984) p. 299
9) H. K. D. H. Bhadeshia, L. E. Svensson, and B. Gretoft: *Acta Metall.,* **33** (1985) p. 1271
10) T. Zacharia, J. M. Vitek, J. A. Goldak, T. A. DebRoy, M. Rappaz and H. K. D. H. Bhadeshia: *Model. Sim. Mater. Sci. Engg.*, **3**, 1995, p. 265
11) J. Ronda and G. J. Oliver: *Comput. Methods Appl. Mech. Engrg.*, **189** (2000) p. 361
12) N. Yurioka: *ISIJ International*, **41** (2001) p. 566
13) P. W. Fuerschbach, G. R. Eisler and R. J. Steele, Proc. of 5th Intl. Conference on Trends in Welding Research, ASM International, Materials Park, OH, USA (1999) p. 488
14) K. Andersen, G. E. Cook, G. Karsai, K. Ramaswamy: *IEEE Trans. Indus. Applications*, **26** (1990) p. 824
15) D. White and J. Jones: *JOM*, **49** (1997), p. 49
16) H. K. D. H. Bhadeshia: *ISIJ International*, **39** (1999) p. 966
17) http://www.sandia.gov/organization/div6000/ctr6500/SmartWeld-picture.html
18) F. Boitout and J. M. Bergheau, Proceedings of symposium on "Joining and Welding Solution to Industrial Innovation," held at Osaka University, Japan on March 14, 2003
19) M. L. Santella, S. S. Babu, B. Riemer, and Z. Feng: Proc. of 5th Intl. Conference on Trends in Welding Research, ASM International, Materials Park, OH, USA (1999) p. 605
20) S. S. Babu, M. S. Summers and G. Sarma: Unpublished research, Oak Ridge National Laboratory, December 2002.
21) E. Gallopoulos, E. N. Houstis, and J. R. Rice: *ACM Computing Surveys*, **27** (1995), p. 277
22) Materials Algorithm Project, http://www.msm.cam.ac.uk/map
23) S. Fukumoto and W. Kurz: *ISIJ International*, **38** (1998), p. 71
24) S. A. David, and J. M. Vitek: Lasers in Metallurgy, Eds. K. Mukherjee and J. Mazumder (Warrendale, PA: The Metallurgical Society, (1982), p. 247
25) N. Suutala: *Metall. Trans. A.,* **13A** (1982), p. 2121
26) J. M Vitek, A. Das Gupta, and S. A. David: *Metall. Trans. A.,* **14A** (1983) p. 1833
27) S. Katayama and A. Matsunawa: Proceedings of Material Processing Symposium, Vol. 44, Laser Institute of America, ICALEO, (1984) p. 60
28) S. S. Babu, S. A. David, and M. A. Quintana: *Welding Journal*, **80** (2001), p. 91s
29) S. S. Babu, J. W. Elmer, S. A. David, M. Quintana: *Proceedings of Royal Society (Mathematical and Physical Sciences) A*, **458** (2002), p. 811
30) S. S. Babu, J. W. Elmer, J. M. Vitek and S. A. David: *Acta Materialia*, **50** (2002), p. 4763
31) B. Sundman, B. Jansson, J. O. Andersson: *Calphad*, **9** (1985) p. 1
32) J. Agren: *ISIJ International* **32** (1992), 291.
33) M. Hillert and L. Hoglund: *Materials Transactions JIM*, **40** (1999), p. 564
34) J. M. Vitek, E. Kozeschnik and S. A. David: *Calphad*, **25** (2001), p. 217
35) J. M. Vitek, S.S. Babu, T. Koseki: Unpublished research, Oak Ridge National Laboratory, 2003.
36) J. M. Vitek, S. A. David, and C. R. Hinman: *Welding Journal*, **82** (2003) p. 10s
37) M. Rappaz, S. A. David, J. M. Vitek, and L. A. Boatner: *Metallurgical Transactions*, **20A** (1989), p. 1125
38) M. Gaumann, C. Bezencon, P. Canalis, and W. Kuz: *Acta Materialla*, **49** (2001), p. 1051
39) J.D. Hunt: *Materials Science and Engineering*, **65** (1984), p. 75
40) J.-W. Park, S. S. Babu, J. M. Vitek, E. A. Kenik, and S. A. David: Unpublished research, Oak Ridge National Laboratory, 2003.
41) N. Saunders, "Ni-Data Information," Thermotech Ltd., Surrey Technology Center, Guidford, Surrey, GU2 5YG, UK, 1998.
42) M. J. Aziz: *J Appl. Physics*, **53** (1982) p. 1158
43) W. Kurz and D. J. Fisher: Fundamentals of Solidification, 4th revised ed. USA: Trans Tech Publications Ltd, Uetikon - Zuerich, Switzerland (1988)
44) S. S. Babu, M. K. Miller, J. M. Vitek, and S. A. David: *Acta Materialia,* **49** (2001) p. 4149